Comparison of helix and wake steering control for varying turbine spacing and wind direction

Taschner, E.; Becker, M.; Verzijlbergh, Remco; Van Wingerden, J. W.

DOI
10.1088/1742-6596/2767/3/032023

Publication date
2024

Document Version
Final published version

Published in
Journal of Physics: Conference Series

Comparison of helix and wake steering control for varying turbine spacing and wind direction

Journal of Physics: Conference Series **2767** (2024) 032023 doi:10.1088/1742-6596/2767/3/032023

Comparison of helix and wake steering control for varying turbine spacing and wind direction

E Taschner[1], M Becker[1], Remco Verzijlbergh[2,3] and JW van Wingerden[1]

[1] Delft Center for Systems and Control, Delft University of Technology, Mekelweg 2, 2628 CD Delft, The Netherlands
[2] Faculty of Technology, Policy and Management, Delft University of Technology, Jaffalaan 5, 2628 BX Delft, The Netherlands
[3] Whiffle Weather Forecasting, Molengraaffsingel 8, 2629 JD Delft, The Netherlands

E-mail: e.taschner@tudelft.nl

Abstract. A variety of wind farm control strategies exist in order to reduce unfavorable wake effects in large wind farms. While strategies like wake steering already reached a high maturity level, it is interesting to compare them to more recently proposed strategies. Such a comparison can form the basis for the development of a symbiotic wind farm control toolbox, from which a control strategy is chosen and activated depending on the operating conditions. The present study compares wake steering with helix control across a wide range of turbine spacings and wind directions using large-eddy simulation (LES). The size of the search space is made computationally tractable for LES by adopting a setup based on one physical upstream turbine and a distribution of virtual downstream turbines which do not exert any thrust force. It is found that helix control is beneficial for full wake overlap and turbine spacing of less than six rotor diameters whereas wake steering proves to be optimal further downstream and for partial wake overlap. Furthermore, the results show that the helix control setpoint in the proximity of full wake overlap scenarios is less susceptible to wind direction variations. This finding indicates that the combination of wake steering and helix control has potential for the design of a wind farm controller which is more robust in full wake overlap scenarios and can reduce the need for large yaw offset adjustments.

1. Introduction

In today's large offshore wind farms unfavorable wake interference induces additional losses in extracted wind power which extend beyond the losses present for a single turbine. To mitigate these wake losses a wide range of wind farm control strategies have been proposed during recent years which can be broadly classified into quasi-steady and dynamic solutions [1]. Quasi-steady solutions include axial induction control to modify the strength of wakes and the steering of wakes using yaw offsets, where control setpoints are only adjusted on a long time scale. In contrast, dynamic solutions like dynamic induction control (DIC) and dynamic wake steering react to changes in operating conditions on much shorter time scale or impose a periodically oscillating actuation around a quasi-steady control setpoint. The latter is the case for the helix, a very recently developed dynamic strategy based on individual pitch control (IPC), which showed promising results when compared to parameterized sinusoidal DIC (the pulse) [2].

The quasi-steady strategies have reached a higher maturity level to a point where for instance static wake steering is available as a commercial product [3]. As more and more control strategies are proposed and progress in maturity the questions arise how the different strategies compare, if they possess different strengths and weaknesses and ultimately if different strategies can be combined. This combination could be a toolbox from which a wind farm controller can choose from depending on the current operating conditions. In principle, this symbiotic approach could either encompass the simultaneous use of different control strategies for the same turbine or a switching logic between them. For example static wake steering and induction control were combined [4] and seminal work compared/combined dynamic wake steering and DIC [5]. The latter study was further extended to compare the two strategies for different farm layouts concluding that aligned and staggered layouts favor wake steering and induction control, respectively [6]. For the third introduced dynamic strategy - the helix - comparisons beyond the pulse control in a full wake overlap scenario are scarce and thus the potential for combination with other control strategies is not well known yet.

The present study explores this potential for the helix and static wake steering control. In the case of a switching logic the identification of the regimes and boundaries within which the different control strategies play to their strength would be crucial as any given constructed wind farm layout can be transformed into a variety of effective aligned/staggered layouts with different turbine spacing by just changing the wind direction. The potential of the helix is conjectured to be maximal in settings of dense turbine spacing and in particular full wake overlap. In these settings the control strategy could be also extended by using a synchronization with downstream turbines [7]. In contrast, these particular settings would require the largest yaw offsets for wake steering, i.e. large deviations from the optimal orientation from a single turbine perspective [8]. Consequently, one can hypothesize that helix and wake steering can be combined into a wind farm control toolbox where each control strategy only operates within its most beneficial regime.

The main contribution of this work is a map that suggests a control strategy and setting based both on the lateral offset and the distance of a neighboring downstream turbine. The map is derived based on turbulent large-eddy simulation (LES) data and distinguishes between three control settings: baseline greedy control, helix control and wake steering control. Extending the map for a range of atmospheric boundary layer (ABL) conditions would then result in a steady state controller, but could also help with wind farm layout optimization using control co-design as shown by [8]. In the subsequent sections we first present the adapted LES methodology for the precursor ABL and the successor turbine simulations before concluding with the obtained map and its implications for the potential of a switching controller.

2. Simulation Methodology

The simulation methodology follows two steps: Firstly, the ABL flow is developed using a precursor simulation. This precursor simulation then provides the inflow for the subsequent successor simulations containing the wind turbine operating with different control strategies.

2.1. Precursor LES simulation: Conventionally neutral ABL (CNBL)

The ABL type is chosen to be a CNBL, i.e. a neutrally stratified boundary layer capped by a strongly stable inversion and a mildly stable free atmosphere aloft (the free lapse rate is $\gamma = 1\,\mathrm{K/km}$). This ABL type is frequently used for LES of wind farms (e.g. [9, 10]) and has been also used previously for an LES study of the helix [11]. Similar to the setup in the latter study the surface roughness is chosen here representative for offshore conditions ($z_0 = 0.0002\,\mathrm{m}$) and the latitude is set to the Dutch North Sea coast ($\phi = 52.6°$). The initial condition (IC) for the vertical potential temperature profile is determined by setting the inversion base height to

$h_0 = 700\,\mathrm{m}$, estimating the required strength of the capping inversion for equilibrium [9] and using the Rampanelli-Zardi model [12].

The desired velocity profile should both attain a wind direction of $\varphi = 270°$ (parallel to the x-axis of the LES domain) and a wind speed of $u_{horiz} = 10\,\mathrm{m/s}$ at a height of $z = 150\,\mathrm{m}$ (the turbine hub height), which places the upstream turbine in the successor simulations at the upper boundary of the control regime II where the rotor speed is still adjusted to track an optimal power coefficient C_P. These requirements are ensured by employing an ABL controller in the precursor which adjusts the direction and magnitude of the driving pressure gradient accordingly. Since the equilibrium solution is an outcome of the chosen ABL setup and thus a priori unknown it is not possible to initialize the velocity with a profile which fulfills the steady geostrophic wind balance (the momentum balance between pressure gradient and Coriolis force above the capping inversion). However, this leads to inertial oscillations of the wind speed and direction above the capping inversion which are not damped as there is no turbulence present above the inversion [9]. Using a geostrophic wind forcing and geostrophic wind speed as IC would not give rise to these oscillations, but does not provide any control of the hub height wind conditions. As a remedy a modified controller was recently proposed which employs damping above the capping inversion [13]. Since this damping essentially resembles a Rayleigh damping layer with dynamically adjusted reference values the present study follows this approach, but adapted in the following way for offline reference input (inspired by [14]).

Initially, the ABL turbulence is developed for eight hours using the ABL controller until the state within the boundary layer is quasi-steady and consequently also the controlled driving pressure gradient. The pressure gradient is then sampled during the following hour and its average is converted into an equivalent geostrophic wind according to $u_g = -1/(f_c\rho)\,\partial\overline{p}/\partial y$ and $v_g = 1/(f_c\rho)\,\partial\overline{p}/\partial x$ [15], where the Coriolis parameter is given by $f_c = 2\sin(\phi)\Omega_z$ ($\Omega_z = 7.29 * 10^{-5}\,\mathrm{rad/s}$) and $\rho = 1.225\,\mathrm{kg/m^3}$ is the reference density. The geostrophic wind speed components are then set as references for a Rayleigh damping layer which spans the free atmosphere and decays to zero in the inversion layer according to a cosine function. The damping factor is chosen as $\alpha = 1$ for a critically damped system [13]. Subsequently the simulation is then continued for twelve hours to dampen the inertial oscillation.

Using the outlined setup and procedure the ABL flow is obtained with the open-source LES code AMR-Wind[1], which solves the filtered incompressible Navier-Stokes equations on block-structured Cartesian grids [16]. The domain size is chosen as $(L_x, L_y, L_z) = (4096, 3200, 1280)\,\mathrm{m}$ giving sufficient space for the development of ABL turbulence and later for capturing a range of wind directions and turbine spacings in the successor simulations. The grid resolution is uniform with $\Delta x_{LES} = 8\,\mathrm{m}$ and the constant time step of $\Delta t = 0.4\,\mathrm{s}$ sets a Courant-Friedrichs-Levy (CFL) number of CFL ≈ 0.6.

Figure 1 (a) shows the development of the horizontal wind speed at four different heights within and above the boundary layer. It can be seen how the wind speed within the ABL reaches a quasi-stationary state while an inertial oscillation manifests for the horizontal wind speed in the free atmosphere where the period is determined by the latitude (i.e. the Coriolis parameter). The Rayleigh damping is active from $t = 8 - 20\,\mathrm{h}$ as can be seen from the mitigated wind speed oscillation at $z = 1100\,\mathrm{m}$. The resulting vertical profiles of horizontal wind speed $\overline{u}_{horiz}$, wind direction $\overline{\varphi}$ and turbulence intensity $\overline{TI}$ (defined based on turbulent kinetic energy) averaged for the time interval $t \in (20 - 20.5)\,\mathrm{h}$ are shown in Figure 1 (b)-(d) across the rotor area. This half an hour interval is the period used as inflow boundary condition for the successor simulations. The variations of TI level and local shear exponent $\alpha = (z/\overline{u}_{horiz})(d\overline{u}_{horiz}/dz)$ across the rotor are $\overline{TI} \in (3, 5)\,\%$ and $\alpha \in (0.07, 0.1)$

[1] `https://github.com/Exawind/amr-wind`

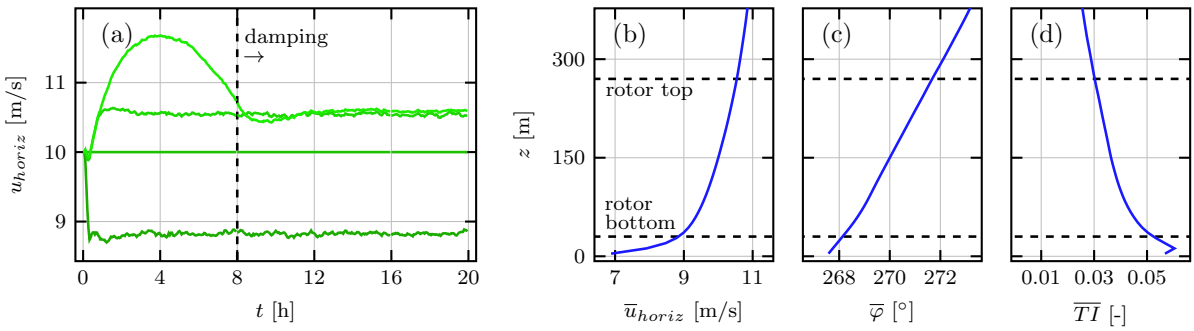

Figure 1. Development of the horizontal wind speed at $z \in (30, 150, 270, 1100)$ m in/above the ABL (darker green for decreasing z), where Rayleigh damping is activated at $t = 8$ h (a). Vertical mean profiles of horizontal velocity (b), wind direction (c) and turbulence intensity (d) averaged across $t \in (20 - 20.5)$ h.

2.2. Successor LES simulations: Greedy baseline, helix and wake steering control

The comparison of wake steering and helix is a high-dimensional optimization problem since the effectiveness of each control strategy depends on the ABL condition and the given wind farm layout. The former point is addressed by choosing a single low turbulence ABL condition since wake control strategies are most likely to be employed therein. To tackle the latter point one requires an approach to reduce the degrees of freedom since a grid search for the optimal static yaw offset $\gamma_{Opt} = \gamma_{Opt}(S_x, \varphi)$ and additional helix/baseline simulations for each combination of streamwise spacing $S_x = \Delta x/D$ (non-dimensionalized with the rotor diameter D) and wind direction φ are only feasible with engineering wake models, however, such a model is not yet available for helix control and thus this study resorts to LES. A brute force LES approach would become computationally prohibitive when comparing an increasing number of (S_x, φ) combinations, but the use of LES can be made tractable by adopting a setup with one physical upstream turbine and a distribution of virtual turbines. The details of this setup are outlined in the following.

The adapted search space for the two control strategies spans the range of turbine spacings $S_x \in (2, 10)$ ($\Delta S_x = 1$) in order to cover the range within wake control might be in principle plausible. The range of wind directions is $\varphi \in (240, 300)°$ at $S_x = 2$ and then decreases monotonously to $\varphi \in (258.2, 281.8)°$ at $S_x = 10$, where at each S_x station the wind direction range is discretized with seventeen points. This ensures that at each streamwise location the angular resolution is maintained in the area of interest, i.e. where wake overlap occurs. The level of wake overlap is also more intuitively given by the so-called view angle ψ which is defined here as the difference between the downstream direction and the wind direction, i.e. $\psi = 270° - \varphi$. Each (S_x, φ) set is the location of a virtual downstream turbine, which does not exert any thrust force. Consequently, given a control actuation at the physical upstream turbine one can estimate the power gain at a waked downstream turbine for all turbine spacings and wind directions with a single simulation. The total simulation count amounts then to one greedy baseline simulation, one simulation per set of helix control parameters and twelve wake steering simulations to discretize the search space of the yaw offsets $N_{Yaw} = (\gamma^+ - \gamma^-)/\Delta\gamma = (30° - (-30°))/5° = 12$. The yaw offset is defined as the difference between the wind direction φ and the turbine orientation θ as $\gamma = \varphi - \theta$. For this study we choose a single set of helix parameters, namely a blade pitch amplitude of $\beta = 3°$ which provides a trade-off between power gain and additional loading [11] and an actuation frequency of $St = 0.3$, where the Strouhal number St is a non-dimensional frequency f defined as $St = f * D/\overline{u}_{hub}$. Thus one can obtain an estimate for the

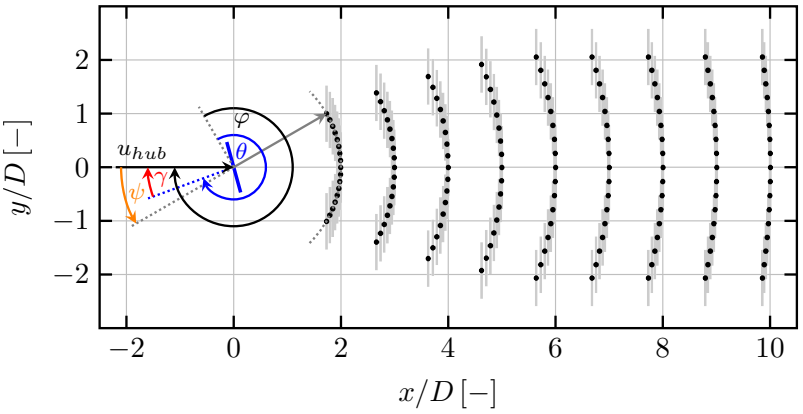

Figure 2. Positions of the physical turbine (blue) and virtual turbines (light gray) together with the definitions of the turbine orientation (blue), wind direction (black), yaw offset (red) and view angle (orange).

optimal control strategy across the entire search space with a total of fourteen simulations. The setup including all angle definitions is also shown in Figure 2.

The physical upstream turbine is modeled using OpenFAST which is a multi-physics wind turbine simulation tool capable of simulating the entire wind turbine including its structural, hydro-, aero- and control dynamics [17] combined with the reference open-source controller (ROSCO) [18]. In this study, the OpenFAST model for the fixed-bottom monopile variant of the IEA-15MW turbine[2] is used. OpenFAST is coupled to the LES simulation using an actuator line model (ALM) [19], where the Gaussian kernel width for the force projection is chosen as $\epsilon = 2\Delta x_{LES}$. Given the still large number of required simulations a grid refinement compared to the precursor simulation is computationally not feasible and thus it is $\epsilon = 16\,\mathrm{m}$. The resulting ratio of LES grid points across the rotor radius is $R/\Delta x_{LES} = 15$ which falls into the category of coarse LES-ALM, which will cause the ALM to overestimate power. To remedy this effect the filtered lifting line correction (FLLC) is employed [20] and the rotor blades are discretized with $N_{Act} = 200$ actuator points, which requires the minimum allowable optimal Gaussian kernel width at the blade tip to be limited to $\epsilon_{Opt} = 1.2\,\mathrm{m}$. The choice of N_{Act} is a trade-off between full convergence of the FLLC at the most outer three percent of the blade and the computational slow down of OpenFAST [21]. For reference a completely resolved FLLC is determined by the chord length c at the blade tip and would require about $N_{Act} \approx 1000$ for the IEA-15MW blade which is not feasible with the constant actuator point spacing employed in OpenFAST ($N_{Act} = R/\min(\epsilon_{Opt}) = R/(0.25\,c_{tip})$). The time stepping further ensures that the CFL condition based on the turbine tip speed is below one. Using these settings the fourteen successor simulations are advanced $T_{Sim} = 30\,\mathrm{min}$ in time, where the first ten minutes are discarded as start-up phase and the latter twenty minutes are the time interval T_A utilized for the analysis.

The last component of the setup is an approach to obtain power estimates of the virtual turbines. The virtual turbines are two-dimensional velocity sampling planes which convert a time series of streamwise velocities $u_x(t, y, z)$ into mean power estimates $\overline{P}_{VT}(S_x, \varphi, C_i)$, where C_i represents the control strategy (greedy baseline C_B, yaw C_Y and helix C_H). Combined with the upstream ALM power estimate $\overline{P}_{OF}(C_i)$ one can then estimate the optimal farm control strategy for a given (S_x, φ) set by calculating the power gain for each C_i:

$$G(S_x, \varphi, C_i) = \frac{\overline{P}_{OF}(C_i) + \overline{P}_{VT}(S_x, \varphi, C_i)}{\overline{P}_{OF}(C_B) + \overline{P}_{VT}(S_x, \varphi, C_B)}. \tag{1}$$

This transfer function is based on the C_P look-up table for the IEA-15MW turbine which is

[2] `https://github.com/IEAWindTask37/IEA-15-240-RWT`

obtained from steady-state blade element momentum (BEM) theory. Since the instantaneous wakes in sheared/veered inflow behind a turbine subject to helix actuation or yaw misalignment show large spatial and temporal variations we employ the concept of the rotor equivalent wind speed (REWS) to better capture this heterogeneity [22]. The REWS is then used for the C_P look-up table operation and the entire transfer function for any virtual turbine is given as

$$u_{REWS}(t) = \sqrt[3]{\frac{1}{A_{Rotor}} \int_{A_{Rotor}} u_x^3(t, y, z)\, \mathrm{d}A}, \tag{2}$$

$$\overline{P}_{VT} = \frac{1}{T_A} \int_0^{T_A} \frac{1}{2} C_P(u_{REWS}(t)) \rho A_{Rotor} u_{REWS}^3(t)\, \mathrm{d}t. \tag{3}$$

3. Results – Identification of optimal control strategies and their sensitivities

Applying the outlined simulation methodology one obtains power gain maps for each control strategy $G(S_x, \psi, C_i)$ (Section 3.1), a map of the overall optimal control strategy and power gain $G(S_x, \psi, C_{Opt})$ (Section 3.2) and insight into the potential of a switching controller (Section 3.3).

3.1. Extracted power: Physical and virtual turbines

The power gain map for each individual C_i is obtained by evaluating Equation 1 for each turbine spacing S_x and wind direction φ. In the case of wake steering the upstream power scaling with the yaw offset angle γ is well described by a cosine law $\overline{P}_{OF}(C_Y(\gamma)) = \overline{P}_{OF}(C_Y(\gamma = 0°)) \cos^{P_p}(\gamma)$ where $P_p = 1.7$. The power loss at the upstream turbine due to the helix actuation is 1.34% which is close to the 1.4% loss found in a study using the same turbine in a similar ABL condition and only slightly smaller Strouhal number $St = 0.25$, but a finer grid of $\Delta x_{LES} = 5\,\mathrm{m}$ and no FLLC [11]. Figure 3 shows the power gain maps for the helix and a selected wake steering case ($\gamma = +20°$) to highlight the fundamental differences between the two control strategies. Wake steering leads to an antisymmetric power gain map with respect to a view angle of $\psi = 0°$ whereas the helix leads to a more symmetric map. Furthermore, the power gain of $G(S_x = 5, \psi = 0°, C_H) = 5\%$ is again found to be close to the observed 5.3% in [11] where also the downstream turbine was modeled with an ALM. This agreement goes to show that the developed physical-virtual turbine setup predicts gains of reasonable magnitude.

3.2. The overall optimal control map

The overall optimal control map is obtained by selecting the highest power gain and associated control strategy for each set (S_x, φ) from the fourteen available individual power gain maps $G(S_x, \psi, C_i)$. The result of this selection process is shown in Figure 4. For wake steering one can observe that the largest yaw offsets become optimal for dense spacing and full wake overlap scenarios. Increasing the turbine spacing S_x or deviating further from a view angle of $\psi = 0°$ then favors successively smaller yaw offsets. However, it is in particular interesting to see how the helix compares to the optimal wake steering solution. The helix maximizes the power gain in a small subspace of the considered search space, e.g. it is favored for full wake overlap ($\psi \approx 0°$) and dense turbine spacing of $S_x < 6$ (the yellow region in the left panel of Figure 4). The resulting optimal power gain map $G(S_x, \psi, C_{Opt})$ (right panel of Figure 4) shows close to a symmetric shape around $\psi = 0°$ with a local minimum at the center. In fact, the potential for maximum power gains is at $(S_x, \psi) \approx (4, \pm 5°)$ achieved by large yaw offsets. Further deviating to larger absolute values for the view angle leads to a smooth transition to baseline greedy control being the optimal strategy. In contrast, this transition is not yet appearing in downstream direction, e.g. at $S_x = 10$ wake steering is still favored against baseline control. This should be seen in the light of the utilized ABL condition with low TI level and a further increase is expected to shift the transition upstream towards smaller S_x.

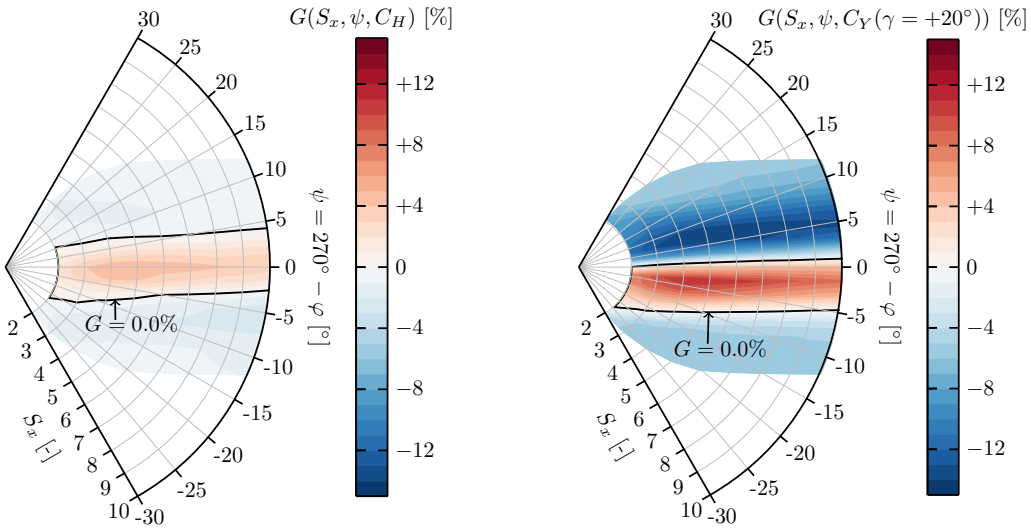

Figure 3. Overall power gain for the helix $G(S_x, \psi, C_H)$ (left) and a selected yaw offset angle $G(S_x, \psi, C_Y(\gamma = +20°))$ (right) as function of turbine spacing and view angle.

3.3. The potential for a switching controller

The introduced map of optimal control strategies is derived for a steady wind direction at hub height, thus any movement in the map due to the in reality varying wind direction is not captured, yet. As soon as $\varphi = \varphi(t)$ the sensitivity of a particular optimal solution for a set (S_x, φ) becomes relevant. To study this idea further assume variations $\Delta\varphi(t) = \pm 5°$ where the turbine controller does not react yet. This means that the turbine orientation is constant which in turn results in induced changes of the yaw offset angle const $= \theta = \varphi(t) - \gamma(t)$. The resulting setpoint change of the upstream turbine can impact the neighboring downstream turbine already after a few minutes while the update period of the controller might be based

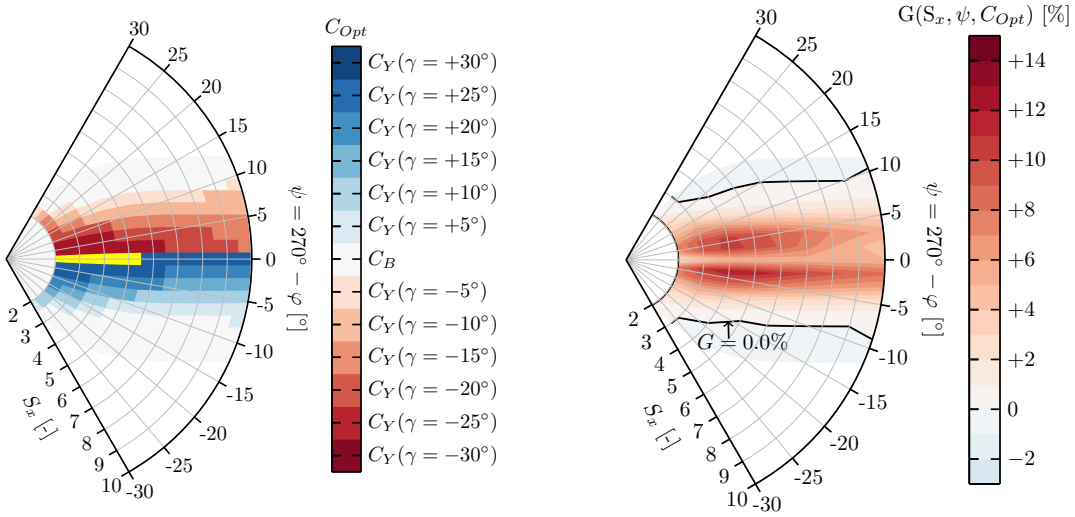

Figure 4. Optimal control strategy C_{Opt} and setting as function of turbine spacing and view angle, where helix control is represented by a yellow region (left) and the respective achievable optimal overall power gain $G(S_x, \psi, C_{Opt})$ (right).

on ten minute averaged data, which essentially means that the turbine array now operates at a different setpoint which can be suboptimal for the new wind direction. Interestingly, even in conditions where the turbine initially only operates with helix control the $\Delta\varphi(t)$ variation will automatically induce a superposed non-zero yaw offset. In order to assess this scenario we perform additional four LES with C_H and small yaw offsets $\gamma \in (-5, -2.5, 2.5, 5)^\circ$ to study the helix performance in the light of a small yaw offset induced by a variation $\Delta\varphi(t)$.

In the following we focus on a spacing of $S_x = 5$. The resulting separate power gain maps for wake steering $G(\varphi, C_Y(\gamma))$ and helix $G(\varphi, C_H(\gamma))$ are shown in the left column of Figure 5. In both plots the black dots indicate the optimal control setpoints for any considered φ bin at $S_x = 5$ (as previously shown in the left panel of Figure 4). These two maps are then further combined to obtain the overall optimal gain $G(\varphi, C_{Opt})$ (top right of Figure 5). It can be seen that helix control increases the achievable gain along the saddle connecting the two power gain maxima in the wake steering map. Furthermore, the discontinuities in vertical direction in the combined map when transitioning from helix to wake steering (indicated horizontal dashed lines) show that an initial control setpoint combining helix and yaw offsets has potential as the overall optimal control strategy for $\psi \approx 0^\circ$. In the present study the combined control is not taken into account for the overall optimization, but is used to assess the sensitivity of the different control strategies in the region of $\psi \approx 0^\circ$ (equals $\varphi \approx 270^\circ$) when moving along the trajectories caused by $\pm\Delta\varphi(t)$ (the three arrows) starting at the respective optimal helix and the two neighboring optimal yaw offset setpoints. The power gain along these trajectories is shown in the bottom right panel of Figure 5 highlighting two key observations. The differences in power gain at $\psi \approx 0^\circ$ are small and trends might change in the light of the approximations made for the simplified LES setup. However, independently of the former observation it can be seen that the helix power gain along the trajectory is more robust than the wake steering solutions, e.g. in order to outperform helix control the wake steering controller has to switch from one extreme setpoint to the other. This requires either significant and timely yaw actuator travel or if not executed due to load, hysteresis or actuator constraints leads to power losses compared to both baseline greedy and helix control. From this analysis one can conclude that helix control could be used to avoid large yaw offsets and could make a wind farm wake steering controller more robust to wind direction variations in full wake overlap scenarios.

3.4. Limitations of the physical-virtual turbine setup

The preceding analysis identifies a potential for a helix-wake steering switching controller. While this is an interesting result, the accurate bounds of regions where a strategy is optimal and the estimate of the power gain are subject to uncertainty due to the made approximations which are summarized here. Firstly, the value of the "correct" extracted power is unknown and both coarse grid LES with an ALM-FLLC and the C_P table look-up approach are expected to deviate from this value. Secondly, wake interaction occurring deeper in the farm, e.g. lateral interaction, helix synchronization and secondary steering effects for wake steering are not captured. Thirdly, the study considers a single low TI CNBL condition with small values of veer.

4. Conclusions

For the first time partial wake overlap scenarios were studied for the helix control approach and were compared to wake steering for a wide range of turbine spacings and wind directions. The qualitatively emerging picture is twofold. Firstly, from a power gain perspective the helix is only competitive with wake steering in full wake overlap scenarios and denser spacing $S_x \lesssim 6$ where exact bounds are subject to the uncertainties summarized in Section 3.4. However, a closer look revealed that independent of the exact optimal gain the helix holds potential for full wake overlap scenarios since it provides more robust power gains in the light of wind direction changes. More importantly it covers this range with a single unmodified control setting while

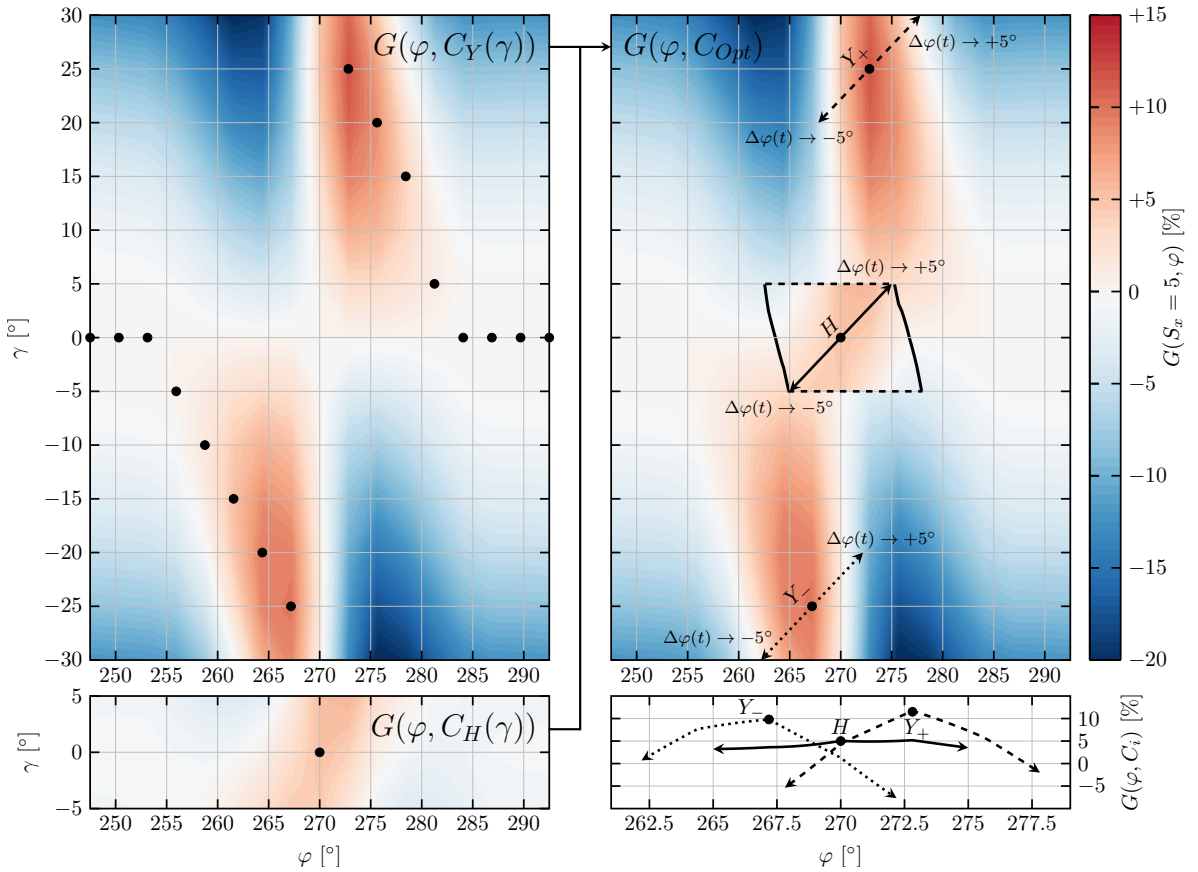

Figure 5. Comparison for $S_x = 5$: Wake steering power gain $G(\varphi, C_Y(\gamma))$ (left top) and helix power gain $G(\varphi, C_H(\gamma))$ (left bottom) as function of wind direction and yaw offset, where black dots indicate the optimal C_{Opt} from Figure 4. Combined map of optimal gain $G(\varphi, C_{Opt})$ with the helix being the optimal strategy within the inset bounded by the solid/dashed black lines (right top) together with the optimal helix ($H\bullet$) and two selected optimal yaw offset setpoints ($Y_-\bullet/Y_+\bullet$). The three arrows indicate trajectories resulting from wind direction variations $\Delta\varphi(t) = \pm 5°$ without any control update ($\theta = \text{const} = \varphi(t) - \gamma(t)$). The right bottom panel shows the power gain $G(\varphi, C_i)$ when starting at the three selected optimal setpoints ($H\bullet/Y_-\bullet/Y_+\bullet$) and moving along the trajectories caused by the wind speed variation $\Delta\varphi(t) = \pm 5°$ (the three arrows in the top right panel).

wake steering might be in principle more favorable, but requiring large yaw offset adjustments of $\Delta\gamma = 50°$. This highlights the potential for a wind farm switching controller.

Finally what this study only touched upon is the simultaneous use of helix and wake steering for the same turbine. In terms of power gain this approach might hold potential while trends for the sensitivity of the gain and turbine loads could be problematic. Anyways it is an interesting question to study the resulting wake dynamics of simultaneous helix-wake steering control.

Acknowledgments

This work is part of the Hollandse Kust Noord wind farm innovation program where CrossWind C.V., Shell, Eneco and Siemens Gamesa are teaming up; funding for the PhDs was provided by CrossWind C.V. and Siemens Gamesa. We further would like to acknowledge the computing

resources provided by DelftBlue [23] and thank SURF for the computational time made available on the Dutch national supercomputer Snellius (grant number: EINF-6784).

References

[1] Johan Meyers, Carlo Bottasso, Katherine Dykes, Paul Fleming, Pieter Gebraad, Gregor Giebel, Tuhfe Göçmen, and Jan-Willem van Wingerden. Wind farm flow control: prospects and challenges. *Wind Energy Science*, 7(6):2271–2306, November 2022.

[2] Joeri A. Frederik, Bart M. Doekemeijer, Sebastiaan P. Mulders, and Jan-Willem van Wingerden. The helix approach: Using dynamic individual pitch control to enhance wake mixing in wind farms. *Wind Energy*, 23(8):1739–1751, 2020.

[3] Siemens Gamesa. https://www.siemensgamesa.com/-/media/siemensgamesa/downloads/en/products-and-services/services/asset-optimization/wake-adapt_en.pdf, last access: 24-01-2024.

[4] Jinkyoo Park and Kincho H. Law. Cooperative wind turbine control for maximizing wind farm power using sequential convex programming. *Energy Conversion and Management*, 101:295–316, September 2015.

[5] Wim Munters and Johan Meyers. Dynamic Strategies for Yaw and Induction Control of Wind Farms Based on Large-Eddy Simulation and Optimization. *Energies*, 11(1):177, January 2018.

[6] Wim Munters and Johan Meyers. Optimal dynamic induction and yaw control of wind farms: effects of turbine spacing and layout. *Journal of Physics: Conference Series*, 1037:032015, June 2018.

[7] Henry Korb, Henrik Asmuth, and Stefan Ivanell. The characteristics of helically deflected wind turbine wakes. *Journal of Fluid Mechanics*, 965:A2, June 2023.

[8] Andrew P. J. Stanley, Christopher J. Bay, and Paul Fleming. Enabling control co-design of the next generation of wind power plants. *Wind Energy Science*, 8(8):1341–1350, 2023.

[9] Dries Allaerts and Johan Meyers. Large eddy simulation of a large wind-turbine array in a conventionally neutral atmospheric boundary layer. *Physics of Fluids*, 27(6):065108, June 2015.

[10] Michael F. Howland, Aditya S. Ghate, Sanjiva K. Lele, and John O. Dabiri. Optimal closed-loop wake steering – Part 1: Conventionally neutral atmospheric boundary layer conditions. *Wind Energy Science*, 5(4):1315–1338, October 2020.

[11] Emanuel Taschner, Aemilius A.W. van Vondelen, Remco Verzijlbergh, and Jan-Willem van Wingerden. On the performance of the helix wind farm control approach in the conventionally neutral atmospheric boundary layer. *Journal of Physics: Conference Series*, 2505(1):012006, May 2023.

[12] G. Rampanelli and Dino Zardi. A Method to Determine the Capping Inversion of the Convective Boundary Layer. *Journal of Applied Meteorology*, 43(6):925–933, June 2004.

[13] Sebastiano Stipa, Arjun Ajay, Dries Allaerts, and Joshua Brinkerhoff. TOSCA – An Open-Source Finite-Volume LES Environment for Wind Farm Flows. *Wind Energy Science Discussions*, 2023:1–41, 2023.

[14] Hugo Olivares-Espinosa and Johan Arnqvist. Modelling of wind turbine wakes over forests along the diurnal cycle. *Journal of Physics: Conference Series*, 2505(1):012043, May 2023.

[15] Roland B. Stull. *An introduction to boundary layer meteorology*. Kluwer Academic Publishers Dordrecht, Dordrecht, 1988.

[16] Lawrence Cheung, Michael J. Brazell, Alan Hsieh, Shreyas Ananthan, Ganesh Vijayakumar, and Nathaniel deVelder. Computation and comparison of the stable Northeastern US marine boundary layer. In *AIAA Scitech 2021 Forum*, Virtual Event, January 2021. American Institute of Aeronautics and Astronautics.

[17] Jason Jonkman. The New Modularization Framework for the FAST Wind Turbine CAE Tool. In *51st AIAA Aerospace Sciences Meeting including the New Horizons Forum and Aerospace Exposition*, Grapevine (Dallas/Ft. Worth Region), Texas, January 2013. American Institute of Aeronautics and Astronautics.

[18] Nikhar J. Abbas, Daniel S. Zalkind, Lucy Pao, and Alan Wright. A reference open-source controller for fixed and floating offshore wind turbines. *Wind Energy Science*, 7(1):53–73, January 2022.

[19] Jens Norkær Sorensen and Wen Zhong Shen. Numerical Modeling of Wind Turbine Wakes. *Journal of Fluids Engineering*, 124(2):393–399, June 2002.

[20] Luis A. Martínez-Tossas and Charles Meneveau. Filtered lifting line theory and application to the actuator line model. *Journal of Fluid Mechanics*, 863:269–292, March 2019.

[21] Emanuel Taschner, Mikko Folkersma, Luis A Martínez-Tossas, Remco Verzijlbergh, and Jan-Willem van Wingerden. A new coupling of a gpu-resident large-eddy simulation code with a multiphysics wind turbine simulation tool. *Wind Energy*, July 2023. Advanced Online Publication.

[22] Frank Scheurich, Peder B. Enevoldsen, Henrik N. Paulsen, Kristoffer K. Dickow, Moritz Fiedel, Alex Loeven, and Ioannis Antoniou. Improving the Accuracy of Wind Turbine Power Curve Validation by the Rotor Equivalent Wind Speed Concept. *Journal of Physics: Conference Series*, 753(7):072029, September 2016.

[23] Delft High Performance Computing Centre (DHPC). DelftBlue Supercomputer (Phase 1). `https://www.tudelft.nl/dhpc/ark:/44463/DelftBluePhase1`, 2022.